Journal of Alloys and Compounds 725 (2017) 941–945

Contents lists available at ScienceDirect

Journal of Alloys and Compounds

journal homepage: http://www.elsevier.com/locate/jalcom

Photoluminescence and phase transition in Er_2O_3 under high pressure

Xiangting Ren [a], Xiaozhi Yan [a], Zhenhai Yu [a], Wentao Li [a, b], Lin Wang [a, *]

[a] Center for High Pressure Science and Technology Advanced Research (HPSTAR), China Academy of Engineering Physics, Shanghai 201203, China
[b] Institute of Atomic and Molecular Physics, Sichuan University, Chengdu 610065, China

ARTICLE INFO

Article history:
Received 31 May 2017
Received in revised form
20 July 2017
Accepted 22 July 2017
Available online 27 July 2017

Keywords:
Rare earth sesquioxides
Hydrostaticity
High pressure
Structural phase transition

ABSTRACT

The phase transitions of Er_2O_3 were investigated using angular dispersive synchrotron x-ray diffraction (AD-XRD) and photoluminescence (PL) spectroscopy at high pressure in different pressure transmitting media. Two successive structural transformations were revealed upon compression. The structural transformation from a cubic *Ia*-3 to a monoclinic *C*2/*m* structure started at 13.6 GPa, and the hexagonal *P*-3*m*1 phase began to appear at approximately 17.8 GPa in helium. Compared with the data in helium, Er_2O_3 showed a much lower onset pressure (6.6 GPa) of the cubic-monoclinic phase transition in silicon oil. The bulk modulus of the cubic phase was obtained from the compression data. The PL measurement indicated that the luminescence lines belonging to the transition of $^2H_{11/2} \rightarrow {}^4I_{15/2}$ and $^4S_{3/2} \rightarrow {}^4I_{15/2}$ of Er_2O_3 were modified under high pressure, which was closely related to the structural phase transition.

1. Introduction

Pressure-induced phase transitions in rare-earth sesquioxides (Ln_2O_3) have evoked increasing attention [1–8]. At ambient conditions, Ln_2O_3 has three polymorphs according to the radius of the Ln^{3+} cation. Larger Ln^{3+} (La-Nd) cation oxides exist in a hexagonal *P*-3*m*1 (A-type) structure. Smaller Ln^{3+} cation (Tb-Lu, Y and Sc) oxides usually crystallize in a cubic *Ia*-3 phase (C-type). Other Ln_2O_3 may exist in both a cubic and monoclinic *C*2/*m* phase (B-type). Considering the pressure effect on the cell volume, the phase transition from C-type to B-type, and even A-type is expected for Ln_2O_3 under high pressure, which has been confirmed in some cases [9,10]. For instance, a pressure-induced C→B phase transition was reported in Yb_2O_3 [2], Sc_2O_3 [10], Er_2O_3 [11,12], and Y_2O_3 [7,8]. The medium cation radii Sm_2O_3 [13] with a mixture of C and B phases was reported to have phase transitions from both C- and B-type to A-type. A C→B→A phase transition sequence was observed in Dy_2O_3 [14], Y_2O_3:Eu^{3+} [7], and Ho_2O_3 [15,16].

Er_2O_3 is widely used in sensing applications such as laser and optical amplifiers [17,18]. The erbium ion (Er^{3+}) is particularly suitable for fluorescence and up-conversion of infrared to visible light due to its favorable electronic level scheme with equally spaced, long-life excited states. In addition, their intrinsic optical properties and applications strongly depend on the grain size and crystalline phase [18,19] of Er_2O_3. Several experimental [1,11,18,20,21] and theoretical studies [4,5] (Table 1) have explored the phase transitions in Er_2O_3. The B type was synthesized in a large volume press (LVP) at 3 GPa and 1020 °C and could be quenched [1]. It should be noted that B-type Er_2O_3 is not thermodynamically stable at ambient pressure and below 2000 °C. Hoekstra's later experiments [20] indicated that the reversible transformation of the C→B type could be realized by annealing the B type in air at 900 °C for several hours. Guo et al. [11] observed a C to B-type phase transition at 9.9 GPa in silicon oil. Theoretical calculations predicted a phase transition from B to A-type at 22 [4] and 19.4 GPa [5]. However, the expected phase transformation from B→A predicted by calculations was not observed in Refs. [11,21]. Er_2O_3 underwent a C to A-type transition in nitrogen [21]. In our previous work [12], we found that nano-Er_2O_3 experienced a C- to B-type phase transition with a partially amorphous structure under compression, which has also occurred in other nanomaterials, such as Gd_2O_3/Er^{3+} nanorods [22], Y_2O_3/Eu^{3+} nanotubes [23], Sm_2O_3 [24], Gd_2O_3 [24], and Y_2O_3 [8,24]. However, these results are not consistent. The reported transition pressures of C→B [5,11] and C→A [5,21] are inconsistent under different hydrostatic conditions. The expected B→A [5,11] phase transformation in Er_2O_3 predicted by calculations has not been observed. The nature of the different transition pressures is still uncertain and whether the calculated evolution of B→A is possible or not remains unclear.

In this work, we investigated the high-pressure behavior of Er_2O_3 using synchrotron x-ray diffraction (XRD) and the photoluminescence (PL) spectrum. We discovered the B→A transition in

---

* Corresponding author.
E-mail address: wanglin@hpstar.ac.cn (L. Wang).

http://dx.doi.org/10.1016/j.jallcom.2017.07.219
0925-8388/

Table 1
Previous studies on the pressure-induced phase transition of Er_2O_3. The C, B, and A denote the cubic, monoclinic, and hexagonal phases of Er_2O_3, respectively. ED-XRD and DFT are short for the energy dispersive x-ray diffraction and Density Functional Theory, respectively.

Method	Transition range/pressure	Transition type	PTM	Ref.
Tetrahedral anvil apparatus	3 GPa, 1020 °C	C→B	pyrophyllite	[1]
	2 GPa, 1273 °C	C→B	pyrophyllite	[20]
ED-XRD	9.9–16.3 GPa	C→B	silicon oil	[11]
	14 GPa	C→A	nitrogen	[21]
DFT	22 GPa	B→A		[4]
	7.05 GPa	C→B		[5]
	19.40 GPa	B→A		
	9.11 GPa	C→A		

Er_2O_3 for the first time. The bulk **modulus** of the cubic phase was obtained from the compression data. The luminescent properties of Er_2O_3 were altered under high pressure. Our results demonstrate that the stability of Er_2O_3 depends on the hydrostaticity.

2. Experimental methods

2.1. Synchrotron AD-XRD and PL spectra under high pressure

A symmetric diamond anvil cell (DAC) with a pair of diamond anvils was used to generate high pressures. The Er_2O_3 sample with a ruby chip was loaded into a sample chamber drilled in a gasket. We used stainless steel (T301) as a gasket. Silicone oil and helium were used as the pressure transmitting media. The pressure was determined by the ruby R1 fluorescence line [25].

The *in situ* monochromatic XRD experiments were performed at beamline 15U1 of the Shanghai Synchrotron Radiation Facility (SSRF). The diffraction patterns were recorded with a charge-coupled device (CCD). The CeO_2 powder was used to calibrate the distance and orientation of the detector. The collected images were integrated into one-dimensional diffraction patterns using FIT2 D software [26]. The structural evolution under high pressure was investigated based on the Rietveld refinements [27] of the integrated patterns.

The luminescence spectra were performed using a Renishaw inVia Raman system with a 532 nm laser beam and a spectrometer with 2400 lines/mm grating giving a resolution of 1 cm^{-1}.

3. Results and discussion

3.1. AD-XRD under high pressure

The crystalline size of the samples in our study was analyzed using SEM. As shown in the low magnification SEM image in Fig. 1, the grain size was in sub-micron scale. We performed **quasi-hydrostatic** compression measurements to elucidate the high-pressure behavior of the sample using helium as a PTM. The structural evolution under pressure was analyzed based on the Rietveld refinements of the integrated diffraction pattern. At ambient conditions, Er_2O_3 crystallized in a cubic structure with space group *Ia*-3 (No.206), 16 molecules per unit cell, and six-fold coordinated Er^{3+}, which is reported in previous literature [11]. As portrayed in Fig. 2, submicron Er_2O_3 was stable in C-type up to 12.0 GPa. When the pressure reached 13.6 GPa, some new peaks belonging to a monoclinic phase emerged, which suggested that the C→B transition started between 12.0 and 13.6 GPa. A typical Rietveld refinement for the mixed phases of the C- and B-type of submicron Er_2O_3 at 14.5 GPa is shown in Fig. 3(a). When pressure increased to 17.8 GPa, the XRD pattern was well characterized by a mixture of C-, B- and A-types phases (seen in Fig. 3(b)), which coexisted up to 19.7 GPa. The C-type disappeared completely at 20.0 GPa, and the B- and A-types coexisted up to 23.5 GPa. Above 25.3 GPa, the submicron Er_2O_3 fully converted to an A-type and remained stable up to the highest pressure. A Rietveld refinement XRD pattern for a pure hexagonal *P*-3m1 phase Er_2O_3 at 29.3 GPa is shown in Fig. 3(c). When the pressure was released, the A-type transformed to a B-type.

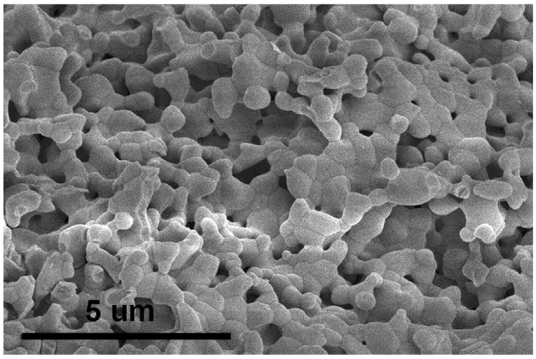

Fig. 1. SEM image of submicron Er_2O_3 at ambient conditions. The scale bar is presented for particle size estimation.

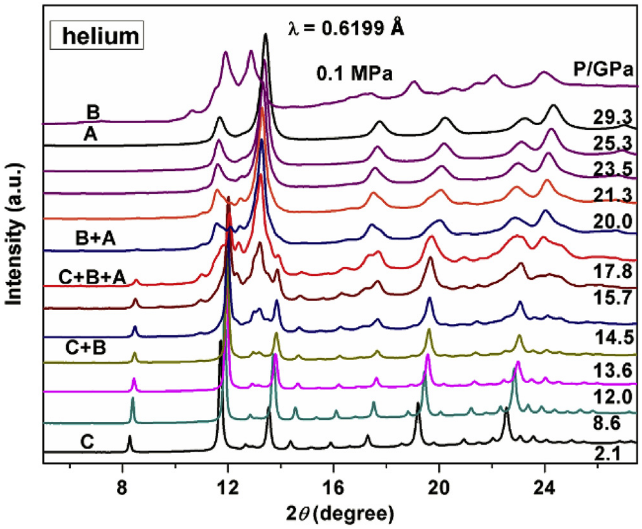

Fig. 2. High-pressure powder XRD patterns of submicron Er_2O_3 in helium.

We also carried out quasihydrostatic compression in silicon oil to confirm the transition route observed in Er_2O_3. As portrayed in Fig. 4, the submicron C-type Er_2O_3 in silicon oil was stable up to 6.6 GPa, when a new weak peak corresponding to the B-type began to appear at 12.6°, and all the XRD peaks shifted to higher 2θ angles upon compression. The intensities of the new peaks increased with

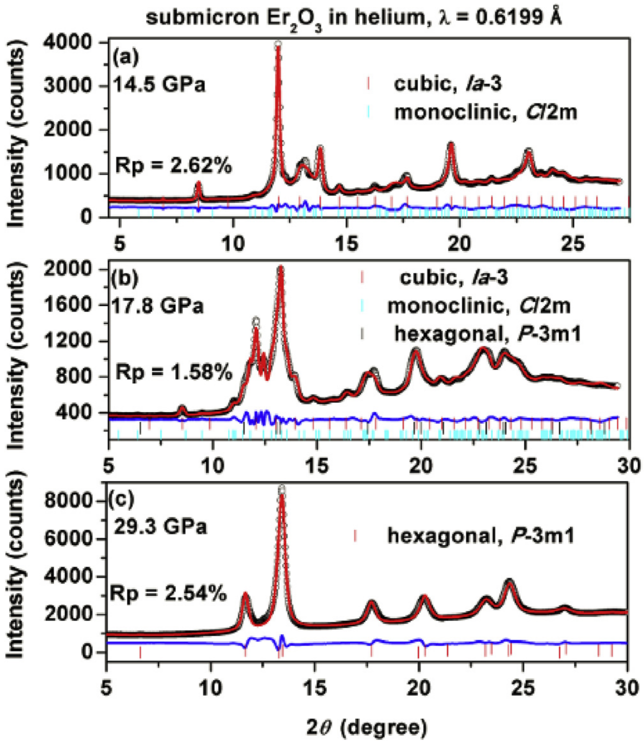

Fig. 3. The representative refinement results of submicron Er$_2$O$_3$ in helium. (a), (b) and (c) are the refinement patterns of submicron Er$_2$O$_3$ under 14.5, 17.8 and 29.3 GPa, respectively. The experimental and calculated data are represented by the black solid sphere and red line. The difference between the observed and the fitted XRD patterns are shown with a blue line at the bottom. The solid short vertical lines show the positions of the Bragg reflections for Er$_2$O$_3$. (For interpretation of the references to colour in this figure legend, the reader is referred to the web version of this article.)

increasing pressure at the expense of the C-type. The peaks of the C- and B-types coexisted up to 12.7 GPa. When the pressure increased to 15.2 GPa, the cubic Er$_2$O$_3$ peaks completely disappeared. When further compressed to 22.5 GPa, some new diffraction peaks appeared that could be indexed to an A-type and increased in intensity. Both the B-type and A-type structure remained stable up to the highest pressure in this study. The top two patterns in Fig. 4 are representative XRD patterns during decompression. The A-type was not quenchable and transformed to a B-type structure that preserved at ambient conditions.

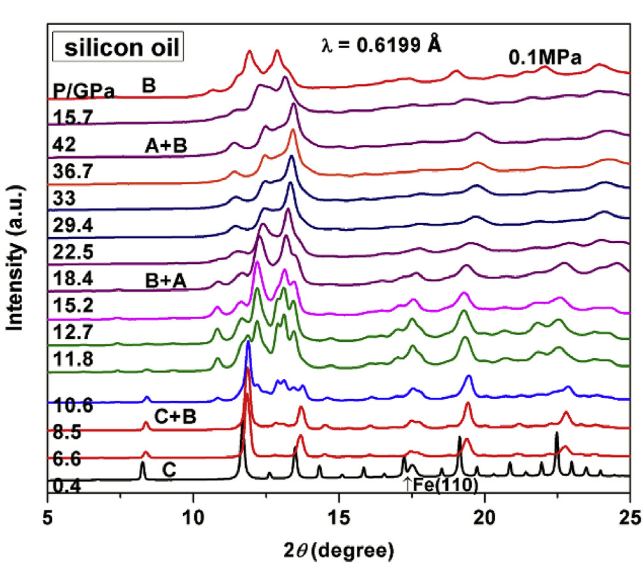

Fig. 4. Selected high-pressure powder XRD patterns of submicron Er$_2$O$_3$ in silicon oil.

It is worth noting that the degree of hydrostaticity affects both the structural stability and transition sequence of Er$_2$O$_3$. Guo et al. [11] suggested submicron Er$_2$O$_3$ underwent a C to B-type phase transition at 9.9 GPa in silicon oil, and the B-type phase was stable up to at least 30 GPa. The onset transition pressure of the C to B-type was higher than that observed in silicon oil and lower than that in helium in this study. Our experimental value in silicon oil (6.6 GPa) is in good agreement with both the high-temperature extrapolation (5 GPa) [20] and theoretically calculated value (7 GPa) [5]. As illustrated in Table 1, Er$_2$O$_3$ underwent a C to A-type transition at 14 GPa in nitrogen [21], while Er$_2$O$_3$ started a C- to B-type transition at 13.6 GPa in helium in this work. We observed the predicted B- to A-type transition at 17.8 and 18.4 GPa, respectively, in helium and silicon oil. Theoretical calculations predicted the B to A-type transition at 22 [4] and 19.4 GPa [5], respectively, which shows good agreement with our results. The onset pressure of the C- to B-type transition was elevated under hydrostatic pressure with a helium pressure medium. Our observed effects of hydrostaticity on the phase transition of Er$_2$O$_3$ in this study agrees with other literature [11,21,28]. We observed a pure A-type Er$_2$O$_3$ in helium for the first time.

Fig. 5 shows the pressure dependent volume of the cubic Er$_2$O$_3$. The pressure-volume data could be fitted to a third-order Birch-Murnaghan equation of state (BM-EoS) [29,30], where B_0 and B'_0 are the bulk modulus and its pressure derivative, respectively. V_0 and V are the volume at ambient condition and pressure P, respectively.

$$P = 3/4B_0[(V_0/V)^{7/3}\text{-}(V_0/V)^{5/3}] \times \{1 + 3/4(B'_0 \text{ - } 4)\ [(V_0/V)^{2/3}-1]\}$$

The bulk modulus of the cubic phase for the submicron Er$_2$O$_3$ in helium are $B_0 = 148.8$ GPa, $V_0 = 73.6329$ Å^3, $B'_0 = 4.02$, respectively. For convenient comparison, we also fitted the pressure-volume data of cubic Er$_2$O$_3$ in silicon oil. The fitting results of our data gave $B_0 = 151.20$ GPa, $V_0 = 73.4189$ Å^3 at fixed $B'_0 = 4$. A comparison

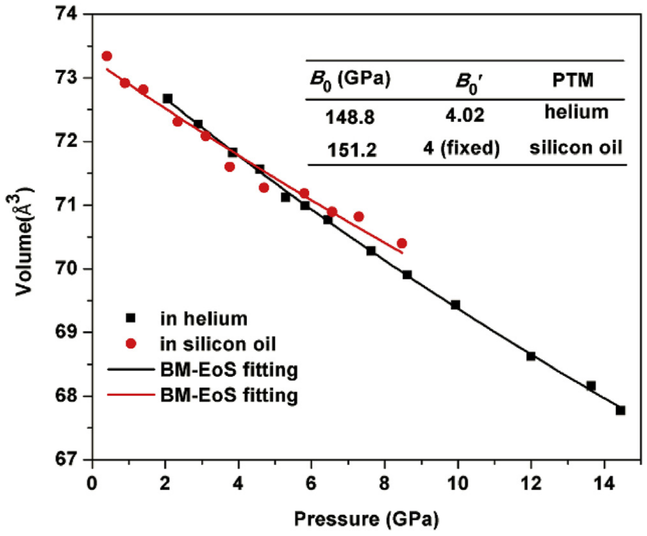

Fig. 5. The variation of the cubic Er$_2$O$_3$ cell volume with pressure. The data in helium and silicon oil are represented with a square and sphere, respectively; the blank and red lines are fitted by the third order Birch-Murnaghan equation of state. (For interpretation of the references to colour in this figure legend, the reader is referred to the web version of this article.)

Table 2
A summary of the bulk modulus (B_0) of cubic Er_2O_3 and their pressure derivative (B'_0) obtained by various methods. PTM refers to the pressure-transmitting medium. BM3 refers to the third-order Birch-Murnaghan equation of state.

Sample	B_0 (GPa)	B'_0	Method and PTM	Ref.
Submicron	148.8	4.02	BM3, helium	This work
	151.2	4 (fixed)	BM3, silicon oil	
Submicron	200(6)	8.4	BM3, silicon oil silicon oil	[11]
Bulk	136	5.9	Vinet, nitrogen	[21]
Nanoparticle	231(3)	4 (fixed)	BM3, silicon oil	[12]
	211(4)	8.4 (fixed)		

between the present results and previously reported data [11,12,21] on the bulk modulus and its pressure derivative is shown in Table 2. The calculated bulk modulus in helium is lower than those of submicron (200(6) GPa) [11] and nanoparticles (211(4) GPa) [12] in silicon oil. Previous works and our present results confirm that: (1) the nanosized samples were harder to compress with a larger bulk modulus than the submicron/bulk samples. (2) The hydrostatic pressure/stress state plays an important role in the measured compressibility, which is consistent with the reported literature [31]. The solidification of silicon oil may have an effect of over-estimating the **bulk modulus**.

3.2. *Photoluminescence of Er_2O_3 under high-pressure*

The luminescence property of materials is determined by their electronic structure, which is closely related to their crystal structure. We performed a high-pressure PL spectroscopy to study the effects of the structural transition on the luminescence properties of Er_2O_3. At ambient conditions, the PL spectra of the submicron Er_2O_3 showed good agreement in both line shapes and wavelength positions with a previous study [32]. The multiplet PL peaks observed from 530 nm to 570 nm originated from the relaxation and emission from $^4S_{3/2} \rightarrow {}^4I_{15/2}$ and $^2H_{11/2} \rightarrow {}^4I_{15/2}$, respectively. Silicon oil was adopted as a PTM. As seen in Fig. 6, no apparent discontinuity, disappearance, or splitting was observed in the luminescence spectra profile below 6.4 GPa for submicron Er_2O_3, indicating that the structure remained stable up to this pressure, which is consistent with our XRD results. When the pressure reached 8.5 GPa, a new peak (labeled with an asterisk) appeared that was attributed to the $^4S_{3/2} \rightarrow {}^4I_{15/2}$ transition accompanying the obvious changes in the relative intensity of the luminescence spectra, and revealing the onset of the structural transition. The bands (labeled with an asterisk) ranging from 545 to 550 nm appeared, which were attributed to the $^4S_{3/2} \rightarrow {}^4I_{15/2}$ transition and became more enhanced at the expense of the original bands completely at 15.3 GPa. In addition, the peaks from the $^2H_{11/2} \rightarrow {}^4I_{15/2}$ transition became gradually weaker and indistinct when the pressure increased further to above 15.3 GPa. The behaviors in the luminescence spectra with increasing pressure indicated a phase transition from cubic to monoclinic. Above 18.1 GPa, a new luminescence peak (arrowed) emerged and its intensity became strong with increasing pressure, combined with a relative intensity change of the two arrowed peaks [33,34], implying a gradual phase transition from monoclinic to hexagonal. The PL spectra only red shifted above 29.9 GPa and remained stable up to 36.7 GPa, the highest pressure. The PL peaks shifted to a shorter wavelength during decompression. The PL peaks of the hexagonal phase were not preserved and transformed to a monoclinic phase after the release of pressure. The pressurized luminescence behaviors in submicron Er_2O_3 were in good agreement with our XRD results and confirmed the related phase transitions of Er_2O_3.

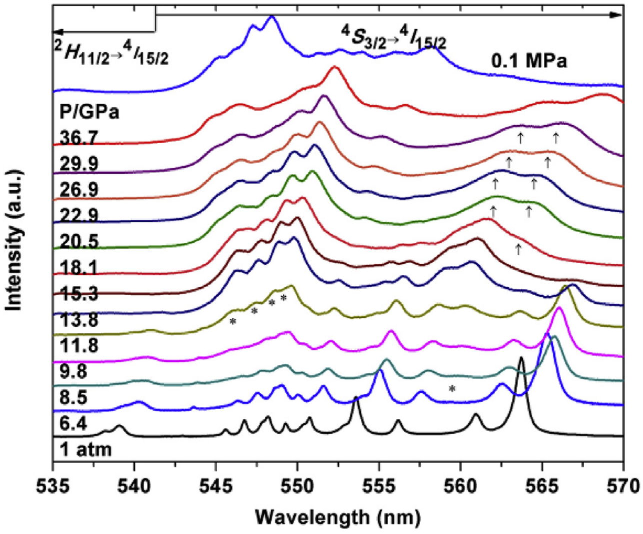

Fig. 6. PL spectra of submicron Er_2O_3 at selected pressures.

4. Conclusions

In conclusion, the high-pressure behaviors of submicron Er_2O_3 were investigated experimentally using AD-XRD and PL spectra techniques in different hydrostatic conditions. Submicron Er_2O_3 experienced C→B→A structural evolutions under high pressure, while the onset transition pressure of cubic Er_2O_3 in silicon oil was much lower than that in helium. By fitting the pressure-volume data of the cubic phase Er_2O_3 in helium and silicon oil, the calculated bulk moduli were $B_0 = 148.8$ GPa, $B'_0 = 4.02$ GPa, and $B_0 = 151.2$ GPa, $B'_0 = 4$ GPa (fixed), respectively. The calculated bulk modulus in helium is lower than that in silicon oil. These results indicate that hydrostatic pressure plays a crucial role in the compression behavior of Er_2O_3 under high-pressure. Moreover, the PL measurements show that the luminescence properties of Er_2O_3 can be altered by the structural phase transition, which aids possible applications in future.

Acknowledgments

We acknowledge the support of the National Science Associated Funding (Grant No. U1530402) and the “Science Challenging Program (Grant No. JCKY2016212A501)”. The authors are also grateful to Ke Yang and Shuai Yan (BL15U1 of SSRF) for their X-ray diffraction measurements.

References

[1] K.A. Hoekstra, H.R. Gingerich, Science (80) 146 (1964) 1163.
[2] C. Meyer, J.P. Sanchez, J.P. Itic, Phys. Rev. B 51 (1995) 187.
[3] H. Chen, C. He, C. Gao, Y. Ma, J. Zhang, X. Wang, S. Gao, D. Li, S. Kan, G. Zou, J. Phys. Condens. Matter 19 (2007) 425229.
[4] B. Wu, M. Zinkevich, F. Aldinger, D. Wen, L. Chen, J. Solid State Chem. 180 (2007) 3280.
[5] Q. Guo, Y. Zhao, C. Jiang, W.L. Mao, Z. Wang, Solid State Commun. 145 (2008) 250.
[6] L. Bai, J. Liu, X. Li, S. Jiang, W. Xiao, Y. Li, L. Tang, Y. Zhang, D. Zhang, J. Appl. Phys. 106 (2009) 73507.
[7] L. Wang, Y. Pan, Y. Ding, W. Yang, W.L. Mao, S.V. Sinogeikin, Y. Meng, G. Shen, H. Mao, Appl. Phys. Lett. 94 (2009) 61921.
[8] L. Wang, W. Yang, Y. Ding, Y. Ren, S. Xiao, B. Liu, S.V. Sinogeikin, Y. Meng, D.J. Gosztola, G. Shen, R.J. Hemley, W.L. Mao, H.K. Mao, Phys. Rev. Lett. 105 (2010) 1.
[9] H.G. Cha, Y.H. Kim, C.W. Kim, D.K. Lee, S.D. Moon, H.W. Kwon, Y.S. Kang, J. Nanosci. Nanotechnol. 6 (2006) 3412.
[10] D. Liu, W. Lei, Y. Li, Y. Ma, J. Hao, X. Chen, Y. Jin, D. Liu, S. Yu, Q. Cui, G. Zou,

Inorg. Chem. 48 (2009) 8251.
[11] Q. Guo, Y. Zhao, C. Jiang, W.L. Mao, Z. Wang, J. Zhang, Y. Wang, Inorg. Chem. 46 (2007) 6164.
[12] X. Ren, X. Yan, P. Wang, Y. Li, S. Wang, F. Peng, L. Xiong, J. Liu, D. He, High. Press. Res. 34 (2014) 70.
[13] S. Jiang, J. Liu, C. Lin, X. Li, Y. Li, J. Appl. Phys. 113 (2013) 1.
[14] S. Jiang, J. Liu, C. Lin, L. Bai, Y. Zhang, X. Li, Y. Li, L. Tang, H. Wang, Solid State Commun. 169 (2013) 37.
[15] S. Jiang, J. Liu, X. Li, L. Bai, W. Xiao, Y. Zhang, C. Lin, Y. Li, L. Tang, J. Appl. Phys. 110 (2011) 2.
[16] X. Yan, X. Ren, D. He, B. Chen, W. Yang, J. Appl. Phys. 116 (2014) 33507.
[17] L.J. Yin, H. Ning, S. Turkdogan, Z.C. Liu, C.Z. Ning, CLEO Sci. Innov. CLEO_SI 2012 1 (2012) 5.
[18] T. Nguyen, C. Dinh, T. Do, ACS Nano 4 (2010) 2263.
[19] S. Heer, K. Kömpe, H.U. Güdel, M. Haase, Adv. Mater. 16 (2004) 2102.
[20] H.R. Hoekstra, Inorg. Chem. 5 (1966) 754.
[21] J.P. Mcclure, PhD Thesis, University of Nevada, Las Vegas, 2009.
[22] X. Yang, Q. Li, Z. Liu, X. Bai, H. Song, M. Yao, B. Liu, R. Liu, J. Phys. Chem. C 117 (2013) 8503.
[23] Z. Li, J. Wang, L. Wang, X. Bai, H. Song, Q. Zhou, T. Wei, D. An, B. Liu, Mater. Res. Express 1 (2014) 25013.
[24] N. Dilawar, D. Varandani, S. Mehrotra, H.K. Poswal, S.M. Sharma, A.K. Bandyopadhyay, Nanotechnology 19 (2008) 115703.
[25] H.K. Mao, J. Xu, P. Bell, J. Geophys. Res. 91 (1986) 4673.
[26] D. Hammersley, A. P, S.O. Svensson, M. Hanfland, A.N. Fitch, Hausermann, High. Press. Res. 14 (1996) 235.
[27] B.H. Toby, H.S. R, A.F. H, B.I. D, R.H. M, U.L. M, U.A. G, U.L. M, U.A. G, U.L. M, U.A. G, EXPGUI, J. Appl. Crystallogr. 34 (2001) 210.
[28] Y. Lin, Y. Yang, H. Ma, Y. Cui, W.L. Mao, J. Phys. Chem. C 115 (2011) 9844.
[29] F. Birch, Phys. Rev. 71 (1947) 809.
[30] F.D. Murnaghan, Proc. Natl. Acad. Sci. 30 (1944) 244.
[31] L. Xiong, J. Liu, L. Bai, Y. Li, C. Lin, D. He, F. Peng, J.F. Lin, J. Appl. Phys. 113 (2013).
[32] J. Cui, G.A. Hope, J. Cui, G.A. Hope, J. Spectrosc. 2015 (2015) 1.
[33] P. Townsend, A. Rowlands, G. Corradi, Radiat. Meas. 27 (1997) 31.
[34] A.P. Rowlands, T. Karali, M. Terrones, N. Grobert, P.D. Townsend, K. Kordatos, J. Phys. Condens. Matter 12 (2000) 7869.